Single-Site Mutations in a Hyperthermophilic Variant of the B1 Domain of Protein G Result in Self-Assembled Oligomers†

Scott C. Meyer, Carmen Huerta, and Indraneel Ghosh*

Department of Chemistry, University of Arizona, Tucson, Arizona 85721

Received August 19, 2004; Revised Manuscript Received November 30, 2004

ABSTRACT: We have characterized two homologous, single-point core mutants of a 57-residue, hyperthermophilic variant of the B1 domain of protein G (HTB1). These single-point mutations in HTB1 replace a Phe residue in the hydrophobic core with either a Glu or Asp residue. Both of these homologous core-variant mutants undergo significant structural rearrangement from the native, monomeric fold and exist as stable soluble oligomeric species of 5 and 30 nm in diameter. Gel-filtration, dynamic light scattering, circular dichroism spectroscopy, fluorescence spectroscopy, along with Congo Red and Thioflavin T binding clearly demonstrated that these core-variants undergo significant structural rearrangement from the native, monomeric ubiquitin fold. The two oligomeric species did not equilibrate over extended periods of time and displayed distinct secondary structures. The larger of the two species was found to possess structural features that are reminiscent of an emerging class of protein assemblies prone to β-sheet-mediated aggregation. These results are significant as there are very few examples of extensive conformational or oligomerization switching brought about by single-point mutations in a stable protein-fold.

Self-assembly or oligomerization is a fundamental organizing force in both biological and nonbiological systems (*1*, *2*) and is observed in the organization of cellular membranes and in the exquisite architecture of viral capsids. Self-assembly has also been implicated in amyloidogenic diseases, where many proteins can form homooligomers that adopt β-sheet-rich fibrillar structure (*3*, *4*). A newly characterized self-assembling structure is that of large spherical oligomers (soluble oligomers) of over 5 nm in diameter, which have been observed in the heterogeneous assemblies identified in small heat-shock proteins, amelogenin and ring domain proteins. The small heat shock proteins, such as αA or αB-crystallin, form conformationally flexible soluble oligomers ranging from 8 to 20 nm (*5*), whereas the amelogenins form larger assemblies of 15−70 nm dependent upon temperature (*6*, *7*). The zinc binding, RING-domain proteins such as BRCA1 assemble into heterogeneous soluble oligomers of 50 nm in diameter, which form functional polyvalent scaffolds for protein presentation (*8*, *9*). More recently, a non-RING-domain zinc binding 98-amino acid E7 viral oncoprotein of HPV16, has been shown to assemble into spherical oligomers of 50 nm in diameter (*10*). On another front, soluble oligomeric intermediates of >4 nm diameter that are implicated in the cellular toxicity of amyloidogenic proteins has also emerged as an active research area (*11*−*14*). Anti-amyloid antibodies have been identified that specifically recognize the common oligomeric β-sheet-rich structure of a variety of self-assembling proteins including amyloid-β, α-synuclein, prion1−35, human insulin, and polyglutamine (*15*). All these recent examples of soluble oligomers point to the need for the continued identification and biophysical characterization of proteins that are capable of assembling into soluble oligomers. In this paper, we present the biophysical characterization of soluble oligomers from two homologous single-point core mutations in a hyperthermophilic variant of the B1 domain of protein G (Figure 1).

The immunoglobulin-binding domain B1 of the streptococcal protein G is one of the most extensively utilized model systems for protein folding and design (*16*−*24*). The B1 domain belongs to the ubiquitin superfamily and contains an α-helix that lies across a four-stranded β-sheet (Figure 1) (*25*, *26*). Gronenborn and co-workers have recently shown that five core mutations in the B1 domain result in the formation of domain swapped tetramers (*27*), whereas four core mutations result in domain swapped dimers (*28*, *29*). Another protein with a similar fold, the B1 domain of protein L, has been shown by Baker and co-workers to form domain swapped dimeric structures (*30*). Regan and co-workers have also identified destabilized mutants of the B1 domain that form amyloid like fibrils (*31*, *32*). However, no spherical oligomers of the B1 mutants or the ubiquitin fold family have been reported to date.

The B1 domain of protein G has been computationally redesigned by Mayo and co-workers to afford a hyperthermostable variant (HTB1) by the incorporation of six mutations (Figure 1), which has resulted in stabilization over the parent by 4.3 kcal/mol. Starting with the HTB1 variant of B1, we created a 5 position core library (Figure 1) in an effort to construct metal-responsive allosteric variants. Our selections with HTB1 surprisingly resulted in the isolation of only two core mutants, where the two selected HTB1 mutants contained either an Asp or Glu at position 31 in

† This work was supported by the donors of the Petroleum Research Fund for a PRF Type G grant, the Research Corporation for a Research Innovation Award, the ADCRC, and the Elsa U. Pardee Foundation.

* Corresponding author: Phone: (520) 621-6331. Fax: (520) 621−8407. E-mail: ghosh@email.arizona.edu.

10.1021/bi048197l CCC: $30.25
Published on Web 01/20/2005

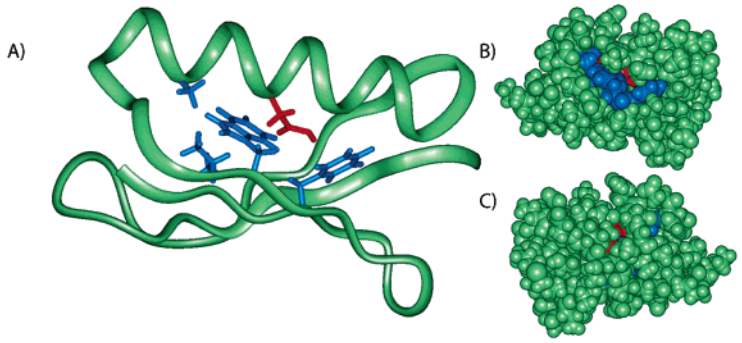

D) **HTB1** TFKLIINGKTLKGEITIEAVDAAEAEKIFKQYANDNGIDGEWTYDDATKTFTVTE
HTB1D TFKLIINGKTLKGEITIEAVDAAEAEKIDKQYANDNGIDGEWTYDDATKTFTVTE
HTB1E TFKLIINGKTLKGEITIEAVDAAEAEKIEKQYANDNGIDGEWTYDDATKTFTVTE

E) **WT B1** TYKLILNGKTLKGETTTEAVDAAEAEKVFKQYANDNGVDGEWTYDDATKTFTVTE
TetB1 TYKVILNGKTLKGETTTEAVDAAEFEKVVKQFFNDNGVDGEWTYDDATKTFTVTE
DimB1 TYKVILNGKTLKGETTTEAVDAAEAEKVVKQFFNDNGVDGEWTYDDATKTFTVTE

FIGURE 1: (A) Ribbon model of HTB1 showing site of the single Glu mutation in red and the randomized residues in blue. (B) CPK model of HTB1 showing site of Glu mutation (red) in same orientation as in A and (C) shows the model rotated by 180° in the plane of the paper. (D) Sequences of HTB1, HTB1D, and HTB1E showing sites of mutation in red and nonmutated sites in blue. The amino acids in bold are the differences between HTB1 and the wild-type B1 (WT B1). (E) The sequences of WT B1, tetrameric (TetB1), and dimeric B1 (DimB1) variants are shown below for comparison. The core mutations are in orange and nonmutated sites in bold.

place of a Phe (Figure 1). Both these mutations arose spontaneously and were not encoded in our starting library, prompting us to further investigate the physical properties of these variants. In the present work, we present circular dichroism, fluorescence, histological dye binding, and dynamic light scattering on the homologous HTB1 core mutants. Our results clearly demonstrate that these single homologous mutations that substitute an acidic residue in place of a buried hydrophobic residue result in the formation of discrete soluble oligomers of either 5 or 30 nm in size. The stable soluble oligomers of 30 nm in diameter are capable of Thioflavin T and Congo Red binding and are reminiscent of an emerging class of proteins that undergo β-sheet-mediated oligomerization.

MATERIALS AND METHODS

HTB1 Library Design and Construction. A phagemid library of HTB1 core mutants was prepared by cassette mutagenesis in the pCANTAB-5E vector containing the HTB1 protein construct (*33*). The parent HTB1 was previously cloned into the pCANTAB vector between the Sfi I and Not I sites, with a unique PstI site incorporated in the sequence allowing for facile cassette mutagenesis. The library-containing cassette was constructed from two overlapping primers that covered the requisite codons corresponding to positions Phe31, Ala35, Trp44, Phe53, and Val55 in HTB1. The synthesized oligonucleotide library contained the NNS mixed codon set for positions 31, 44, 53, and 55, and the SHC mixed codon set for position 35, where N corresponds to either G, C, A, or T; S corresponds to G or C; and H corresponds to either A, T, or C. The primers were designed and obtained from IDT.

Forward primer: gctgatgctgcagaagctgaaaaaatcnnsaaacagtacshcaacgacaacggtatcgacggtgaannsacctacgacgacgctaccaagacc

Reverse primer: gcatagtctagcggccgcttcggtsnnggtsnnggtcttggtagcgtcgtcgtagg

The primers were extended to the full duplex by mutually primed synthesis utilizing the Klenow fragment of *Escherichia coli* DNA polymerase I. The insert was purified and subsequently digested with Not I and Pst I and cloned into a pCANTAB-5E vector containing the digested parent HTB1. After electroporation of XL-1 blue cells, the total library size was 6.3×10^6. During the course of ongoing metal and small molecule binding experiments, two phagemid clones were repeatedly identified that corresponded to spontaneous mutations of either Glu (HTB1E) or Asp (HTB1D) at position Phe31. The repeated identification of these two homologous single-point mutations lead us to further investigate their structure.

Cloning, Expression, and Purification of HTB1, HTB1D, and HTB1E. The parent HTB1 and selected mutants HTB1D and HTB1E were PCR amplified out of pCANTAB-5E using designed primers with appropriate restriction sites and an N-terminal Genenase cleavage site for cloning into the 6xHis-tag expression vector pQE-30. The designed primers were obtained from IDT.

Forward primer: cgcggatccgcagctcattatatgaccttcaagcttatcatcaac

Reverse primer: gtatctcccgggctattcggtaacggtgaaggttttg

HTB1, HTB1D, and HTB1E were then grown in XL-1 Blue *E. coli* and induced with 1 mM IPTG (isopropyl D-thiogalactoside). The soluble fraction from the cell lysate was bound to nickel agarose resin in a 50 mM Na_2HPO_4 and 300 mM NaCl buffer at pH = 8.0. The proteins were then washed and eluted with increasing imidazole concentrations, with the mutants eluting at 500 mM imidazole. The IMAC purified proteins remained clear for > 2 months at room temperature or at 4 °C. Gel filtration chromatography was carried out on Superdex 75 HR 10/30 or a Superdex 200 HR 10/30 column attached to an Amersham FPLC system, in 20 mM Tris-HCl and 150 mM NaCl at pH = 7.4 at 100 μM to 2 mM protein concentrations.

Genanase Cleavage. The alternate conformation of the core mutations does not allow for Genenase-mediated cleavage of the His-tag at all conditions attempted, whereas the parent HTB1 is easily cleaved. Thus, all biophysical studies were conducted in the presence of the His-tag for all studied proteins, including HTB1, HTB1E, and HTB1D.

The His-tag and Genenase cleavage site adds the amino acids MRGSHHHHHHGSAAHY-MAQ before the amino acid sequences shown in Figure 1.

MALDI Mass Spectroscopy. MALDI mass spectra were acquired on Bruker Reflex-III MALDI/TOF. Purified protein samples were dissolved in 50% CH_3CN in H_2O with 0.1% TFA that contained either sinapinic acid or 2,5-dihydroxybenzoic acid as the matrix.

Dynamic Light Scattering. Dynamic light scattering (DLS) data of the mutants were recorded at 25 °C in 20 mM Tris-HCl and 150 mM NaCl (pH = 7.4) on a Malvern Instruments Ltd. Zetasizer 3000HS. The concentration of the each sample was 15−30 μM; no adjustment of concentration was carried out after gel filtration purification. Concentration was calculated by taking the absorbance at 290 nm of a 1:10 dilution in 8 M guanidine-HCl using the calculated molar absorptivity of 9530 $M^{-1}cm^{-1}$. The absorbance spectra of both a heated (95 °C, 10 min) and nonheated samples were taken in triplicate.

Circular Dichroism Spectroscopy. Circular dichroism measurements of HTB1, HTB1E, and HTB1D were taken at 15−30 μM on a Aviv 62A-DS spectropolarimeter with a 0.1-cm path length in 20 mM Tris-HCl, 150 mM NaCl at pH = 7.4 and 25 °C. The proteins were neither diluted nor concentrated prior to acquisition of the spectra, and concentrations were calculated as discussed above. The mean residue ellipticity (MRE) = (θ * 10^3/(0.1 cm * [P] * n), where n is the number of residues, [P] is the monomer protein concentration (μM), θ is in units of (degree * cm^2/dmol), and the spectra were acquired in a 0.1 cm path length cell.

Fluorescence Spectroscopy. Fluorescence emission spectra were taken on a Photon Technology International (PTI) spectrofluorometer with an excitation wavelength of 290 nm. The excitation and emission slit widths were 2 and 4 nm, respectively. Measurements were taken at 15−30 μM in 20 mM Tris-HCl and 150 mM NaCl at pH = 7.4 and 25 °C. The fluorescence intensity was adjusted for concentration of protein present in the sample.

Thioflavin T Binding. 15−30 μM solutions of HTB1, HTB1E, and HTB1D in 20 mM Tris-HCl and 150 mM NaCl (pH = 7.4) were added to a thioflavin T solution for a final concentration of 5 μM protein and 25 μM thioflavin T. A 25 μM sample of aggregated β-amyloid (1−40) was used as a reference standard. Readings were immediately taken on the Photon Technology International (PTI) spectrofluorometer with an excitation at 446 nm (4 nm excitation and 8 nm emission slit widths). The fluorescence intensity was adjusted for concentration of protein present in the sample.

Congo Red Binding. To 900 μL of 15−30 μM solutions of the HTB1 mutants in 20 mM Tris-HCl and 150 mM NaCl (pH = 7.4) was added 100 μL of a 50 μM Congo Red solution in PBS with 10% ethanol. Readings were taken after 30 min on a UV−Vis spectrometer. All readings were compared to a blank of Congo Red prepared in the same buffer system as the other samples.

RESULTS

Identification of HTB1 Variants. During ongoing studies involving the identification of small-molecule binding core mutants of HTB1, two homologous single-point mutants

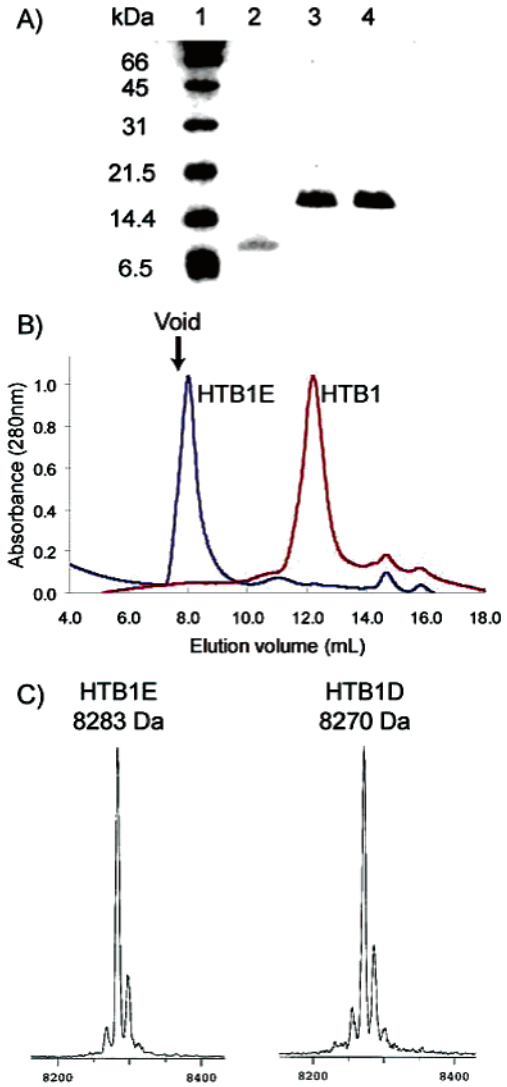

FIGURE 2: Physical characterization of HTB1E and HTB1D. (A) Denaturing SDS−PAGE analysis of HTB1 (lane 2); HTB1E (lane 3), and HTB1D (lane 4) with molecular weight markers in lane 1. (B) Gel-filtration chromatography of HTB1 and HTB1E on a Superdex 75 HR 10/30 column. (C) MALDI mass spectrum of HTB1E and HTB1D.

corresponding to either GAG or GAC codons in place of the original TTC codon of Phe31 in the parent HTB1 were repeatedly identified. Interestingly, besides mutations at amino acid position 31, the codon usage at all other randomized sites corresponded to the parent HTB1. Since our starting library does not incorporate the observed codons, this suggests that the mutations corresponding to Phe31 to either Glu31 (HTB1E) or Asp31 (HTB1D) were spontaneous and presented an opportunity for careful physiochemical characterization.

Physical Characterization of Core Mutants: SDS−PAGE, Gel Filtration Chromatography, MALDI Mass Spectrometry, and IgG binding. HTB1E and HTB1D were both easily expressed (36 mg/L) and purified from the soluble fractions of XL-1 blue cells after sonication. Interestingly, neither protein was observed in the insoluble fractions, which would have indicated possible aggregation driven inclusion body formation. Upon purification by metal-chelate chromatography over a Ni-NTA column, both HTB1E and HTB1D were found to migrate anomalously by SDS−PAGE (Figure

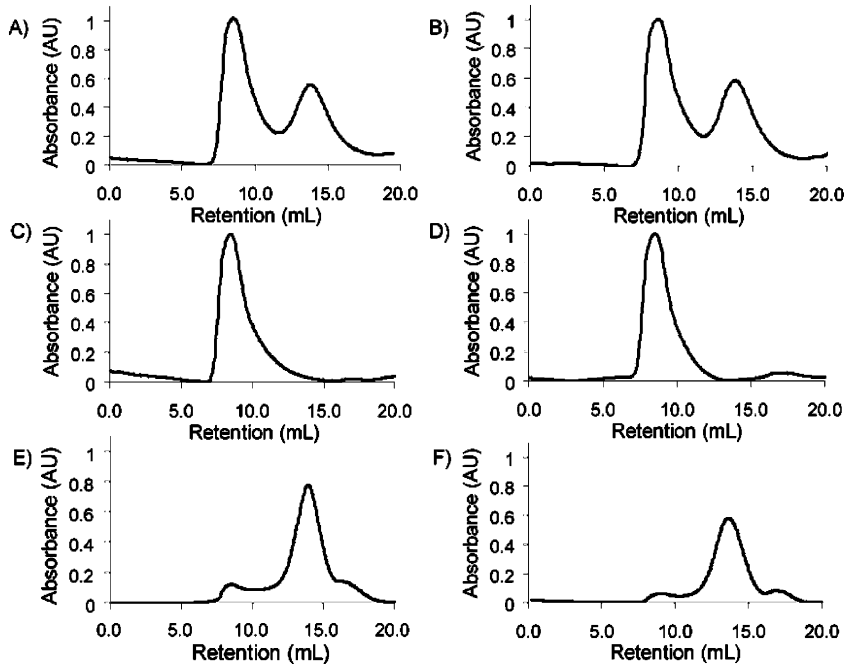

FIGURE 3: Size exclusion chromatography of HTB1E and HTB1D. The core mutants HTB1D (A) and HTB1E (B) were purified on a Superdex 200 HR 10/30 size exclusion column. After 1 week, none of the isolated species (HTB1D peak1 (C), HTB1E peak1 (D), HTB1D peak2 (E), and HTB1E peak2 (F)) reequilibrated to the corresponding species.

2A) in comparison to the parent HTB1 protein. It was hypothesized that the mutants could possibly correspond to a dimeric species. However, when the IMAC-purified HTB1E or HTB1D was subjected to gel filtration on a Superdex 75 column with a molecular cutoff of 70 000 Da, a single peak eluting at the void volume was observed, whereas the parent HTB1 eluted as a monomer (Figure 2B). The elution in the void volume suggested that HTB1E and HTB1D were larger than 70 000 Da rather than the putative dimeric species observed by SDS−PAGE; however, prolonged centrifugation at 6000*g* did not result in any observable precipitation. The absence of any oligomer below 70 000 Da suggests that dissociation constant for the oligomerization of HTB1E and HTB1D must be below the micromolar concentration employed during repeated gel filtration trials. Both proteins were further characterized by MALDI mass spectrometry to verify their molecular weight and were found to correspond to their predicted molecular mass (Figure 2C).

Since these HTB1 variants contain His-tags, we attempted to cleave the His-tag with Genanase. Interestingly, Genanase easily cleaves the His-tag attached to the N-terminus of HTB1, but the His-tags for both HTB1E and HTB1D could not be cleaved under all conditions attempted. This lack of Genanase cleavage suggested that HTB1E and HTB1D exist in a significantly different conformation than HTB1. To eliminate artifacts from the His-tag, HTB1 containing the His-tag was used as a control for all subsequent experiments. We also probed the capability of HTB1E and HTB1D to bind the Fc portion of IgG by a functional test developed by Hellinga and co-workers. HTB1(Cys33) labeled with a acrylodan binds the Fc region of IgG resulting in a strong increase in fluorescence (*34*, *35*). Control competition experiments showed that 30 μM HTB1 could out compete acrylodan-labeled-HTB1(Cys33) (5 μM) bound to Fc (3.5 μM). Utilizing this assay, we found that neither core mutants HTB1E or HTB1D had any measurable effect upon the acrylodan-labeled-HTB1−Fc complex at up to 30 μM concentrations (Supporting Information). These results all pointed to significant structural rearrangement of HTB1 upon a single-point core mutation.

Gel-Filtration Chromatography. To further characterize the oligomeric species of both HTB1E and HTB1D, we employed a gel-filtration column with a larger molecular weight cutoff (700 000 Da) and successfully separated two oligomeric species (Figure 3 A,B). The relative ratios of the oligomeric species corresponding to peak1 (HTB1Ep1) and peak2 (HTB1Ep2) of HTB1E were found to be 1.6:1, whereas the relative ratios of the peaks corresponding to peak1 (HTB1Dp1) and peak2 (HTB1Dp2) of HTB1D were found to be 1.4:1. After separation of the sample, the peaks corresponding to the two oligomers, either HTB1Ep1 and HTB1Ep2 or HTB1Dp1 and HTB1Dp2 were stored at room temperature and analyzed after 1 day or 1 week. Upon reinjection of the samples we found that there was almost no observable equilibration of the two distinctly sized oligomeric species under our experimental conditions (Figure 3C−F). To further investigate the relative ratios of the two peaks, we refolded HTB1E at four different concentrations from 50 to 200 μM, and quite surprisingly, we did not observe a concentration-dependent preference for either of the two observed oligomeric species (Figure 4). The relative ratios of HTB1Ep1 and HTB1Ep2 were found to be constant under these conditions, suggesting that these oligomers may arise from distinct folding pathways that are equally concentration dependent.

To estimate the molecular weight of the two species, we generated a standard curve utilizing protein molecular weight standards (Supporting Information). The smaller of the two species, HTB1Ep2 and HTB1Dp2, were found to elute at molecular masses corresponding to 75 000 and 83 000 Da, respectively, assuming similar volumes to the standards. However the larger peak, HTB1Ep1 and HTB1Dp1, eluted in the void volume of the column that suggests a molecular mass larger than 700 000 Da (Table 1).

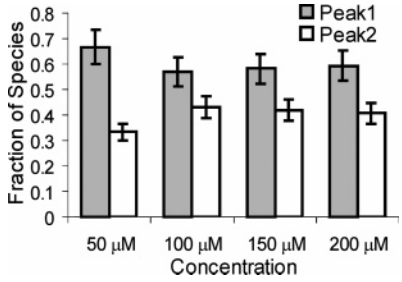

FIGURE 4: Concentration dependence of oligomer distribution during protein refolding. HTB1D was refolded at various concentrations and the resulting samples were analyzed by gel filtration chromatography. Peaks corresponding to HTB1Dp1 (gray) and HTB1Dp2 (white) were integrated and compared to obtain a relative ratio of the two oligomeric species.

Table 1: Molecular Weight Determination via Gel Filtration Chromatography

protein	peak 1 (kDa)	peak 2 (kDa)	native (kDa)
HTB1			8.3
HTB1E	>700	75	
HTB1D	>700	83	

Dynamic Light Scattering. To further study the oligomerization properties of these mutants, we turned to DLS, which provides a convenient measure of particles in the 10 nm to 5 μm regime and has been an useful method for studying large soluble oligomers of β-amyloid, small heat-shock proteins, ring-domain proteins, β-lactoglobulin, and the E7 protein of HPV-16. DLS clearly showed (Figure 5) that the soluble oligomers of both HTB1D and HTB1E form significantly large particles with two distinct size ranges that agree well with the results from gel-filtration chromatography. HTB1Ep1 has an average diameters centered at 34 nm and HTB1Ep2 has an average diameter centered at 5.6 nm. Samples containing HTB1Dp1 showed similar size distribution to HTB1Ep1, with a average diameter of 25 nm, whereas HTB1Dp2 was very similar in size to HTB1Ep2 with a diameter of 5.1 nm. DLS data was also acquired for freshly dialyzed samples of HTB1D and HTB1E along with samples left standing at room temperature over a 4-week period and showed no change in size or oligomer distribution by DLS or gel-filtration chromatography. These results suggest that these soluble particles do not undergo time-dependent aggregation that is often observed in proteins prone to amyloidogenesis.

Circular Dichroism Spectroscopy. Both oligomeric species for HTB1D and HTB1E were characterized by far-UV CD spectroscopy to establish whether the secondary structure of HTB1E and HTB1D was significantly different than that of the parent HTB1 protein (Figure 6). The CD spectra of peak2 of HTB1E and HTB1D both appear to be less structured than the parent HTB1 protein as indicated by a 65% lower overall mean residue ellipticity at 222 nm compared to the parent HTB1. In comparison to peak2, the large soluble oligomer corresponding to peak1 of HTB1D and HTB1E both display significant minima at 218 nm, suggesting considerable β-sheet structure. Compared to peak1, peak2 for both HTB1D and HTB1E appears to be less structured. Thus, both proteins with single residue mutations form two discrete soluble aggregates that appear to possess distinct secondary structure.

Fluorescence Spectroscopy. The parent HTB1 and our two variants contain a single tryptophan at position 44, which is partially buried in the native structure (Figure 1). This tryptophan provides a sensitive conformational probe for comparing the relative burial of this residue in the three proteins (Figure 7). The fluorescence emission spectra of the two oligomeric species of HTB1E and HTB1D clearly show that the tryptophan environment is distinctly different with an emission maximum centered at 348−349 nm for the smaller oligomers and at 344−345 nm for the larger oligomers based upon center of spectral mass (Table 2). When compared to the tryptophan emission spectra of the parent HTB1 protein (348 nm), the emission spectra corresponding to peak2 of both HTB1D and HTB1E mutants appear to be similar (Figure 7) but considerably quenched, possibly by the nearby acidic mutation. In comparison to peak2, the tryptophan emission in the larger oligomers, corresponding to HTB1Dp1 and HTB1Ep1, is blue-shifted by 5 nm. This blue shift points to a more buried environment that is consistent with the increased β-sheet structure seen in the circular dichroism spectra.

Thioflavin T and Congo Red Binding. The increase in thioflavin T fluorescence emission upon excitation at 446 nm is a sensitive probe for aggregated β-sheet structure and is the method of choice for following in vitro amyloid

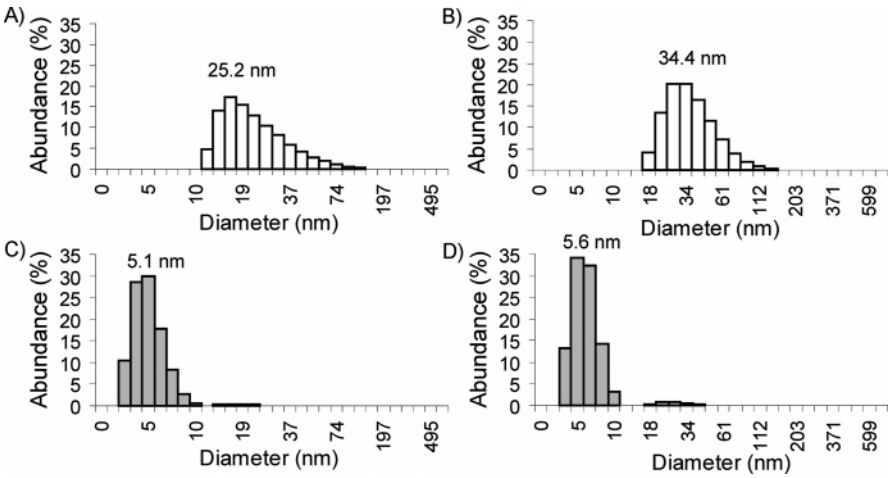

FIGURE 5: Dynamic light scattering of HTB1D and HTB1E. The volume-based populations of the isolated HTB1Dp1 (A), HTB1Ep1 (B), HTB1Dp2 (C), and HTB1Ep2 (D) are shown as determined by dynamic light scattering.

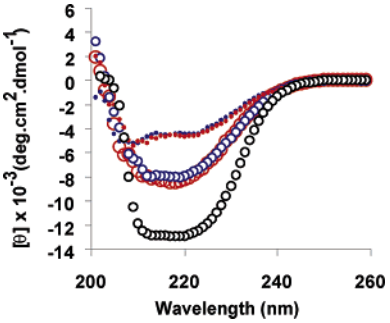

FIGURE 6: Far UV circular dichroism of HTB1D and HTB1E species. The CD spectra of HTB1Dp2 (small red circles), HTB1Dp1 (large open red circles), HTB1Ep2 (small blue circles), and HTB1Ep1 (large open blue circles) are shown with HTB1 (open black circle).

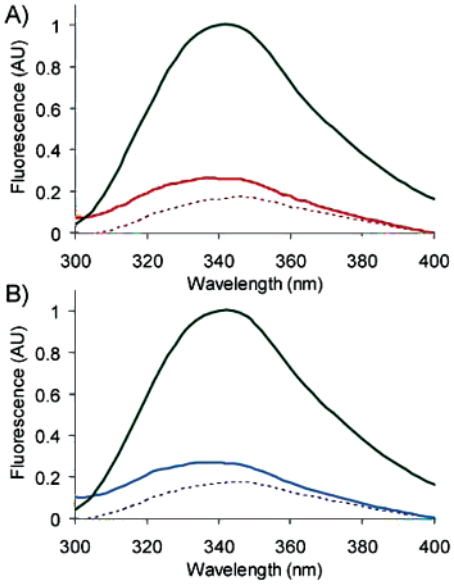

FIGURE 7: The tryptophan fluorescence of HTB1D and HTB1E. (A) HTB1Dp1 (solid red), HTB1Dp2 (dashed maroon) tryptophan fluorescence spectra compared to HTB1 (solid green). (B) HTB1Ep1 (solid blue) and HTB1Ep2 (dashed blue) compared to HTB1 (green). The excitation wavelength for all experiments was 290 nm.

Table 2: Center of Spectral Mass[a]

protein	peak 1 (nm)	peak 2 (nm)	native (nm)
HTB1			348
HTB1E	344	349	
HTB1D	345	349	

[a] Center of spectral mass was calculated as $\langle \nu^* \rangle = \Sigma(\nu_i F_i)/\Sigma(F_i)$ were F is the fluorescence intensity at a given wavelength (ν) over the range $300 < \nu < 400$ nm.

aggregation. Similarly, the shift in absorbance in Congo Red also provides proof of β-sheet rich amyloid-like secondary structure. To further study the structure of our mutants, we turned to thioflavin T fluorescence and Congo Red absorbance changes as it has been utilized for the spherical aggregates of the E7 protein of HPV-16 (*10*) and β-lactoglobulin (*36*). We envisioned that in our HTB1 mutant system, β-sheet-mediated higher-order self-assembly might be a reasonable pathway for the HTB1E and HTB1D to self-assemble into the larger oligomeric assemblies. Both HTB1Dp1 and HTB1Ep1 showed similar ThT dependent fluorescence that was significantly stronger than the parent

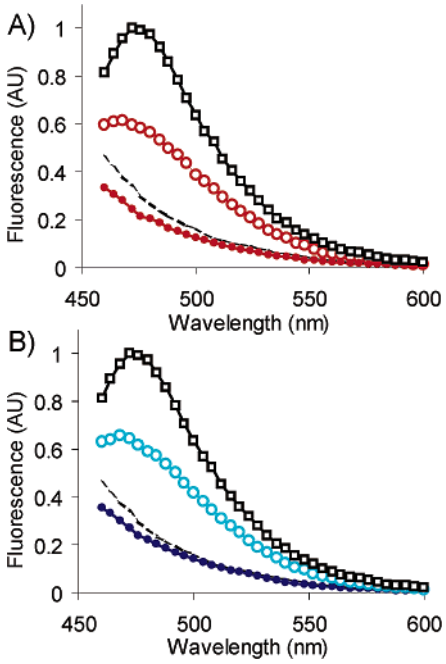

FIGURE 8: Thioflavin T binding of HTB1D and HTB1E. Thioflavin T-dependent fluorescence emission of (A) HTB1Dp1 (open red circles), HTB1Dp2 (solid red circles) as compared to HTB1 (dashed black) and β-amyloid (black squares). Thioflavin T fluorescence of (B) HTB1Ep1 (open blue circles), HTB1Ep2 (solid blue circles) with HTB1 (dashed black) and β-amyloid (black squares). Thioflavin T-dependent emission was monitored by excitation of 446 nm.

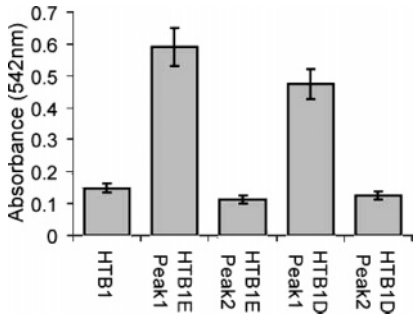

FIGURE 9: Congo Red binding. The graph shows the relative increase in absorbance at 542 nm of each added oligomeric species in comparison to Congo Red in buffer alone.

HTB1 and ThT controls (Figure 8). Furthermore, the change in fluorescence for both of the larger oligomers was similar to that observed for a β-amyloid (1−40) fibrillar preparation used as a control. In comparison to the larger soluble oligomers, the smaller oligomers corresponding to HTB1Dp2 and HTB1Ep2 did not show thioflavin T binding, thus pointing to distinct structural features for these species. The change in Congo Red absorbance (Figure 9) followed similar trends as the thioflavin T fluorescence changes, in that the larger oligomers, HTB1Ep1 and HTB1Dp1, clearly bind Congo Red, whereas the smaller oligomers show no appreciable Congo Red binding as compared to the parent HTB1.

DISCUSSION

The B1 domain of protein G is one of the most extensively characterized proteins and has served as the testing ground for numerous studies in protein folding and design. The B1

domain has been computationally redesigned to a hyperthermostable variant (HTB1) by the incorporation of six core mutations. Starting with the HTB1 variant of B1, we have recently created a core library of all 20 amino acids in an effort to construct metal sensitive variants. The selection of HTB1 variants from a 6.3×10^6 member library surprisingly resulted in only two homologous mutants at position 31 that arise from spontaneous mutations in the parent HTB1 protein and are not encoded in our library. Spontaneous mutations have often been observed in phage display (*37*). However, the physical origins of the selective advantage of the mutants, HTB1E or HTB1D, over the parent HTB1 are not apparent. What is remarkable is that both spontaneous mutations are at the same site and only code for the homologous amino acids, Asp and Glu, in place of the original core Phe residue. This observation prompted further biophysical evaluation of the selected HTB1 core mutants.

We found that both the Glu (HTB1E) and Asp (HTB1D) core mutants of HTB1 were overexpressed in the soluble fractions at the same levels as the parent hyperthermophilic parent, HTB1, and were not observed in insoluble inclusion bodies as is the case with aggregation prone de novo designed proteins that predominantly form β-sheets (*38*). Furthermore, the anomalous migration of HTB1E and HBT1D in SDS gels suggested the possibility that these mutants could perhaps undergo domain swapping as observed for GB1 core variants (*27*, *28*, *39*) and in the B1 domain of protein L (*30*, *40*). However, gel filtration chromatography and DLS clearly established that the oligomers of HTB1E and HTB1D do not exist as stable dimers but as two distinct sizes of large oligomers that are either 5 nm in diameter or between 20 and 40 nm in diameter.

Careful separation of the two oligomeric species by gel filtration allowed us to fully characterize the physical properties of these core mutants. The smaller of these oligomers, HTB1Ep2 and HTB1Dp2, had an average size that corresponds to 70 000−80 000 Da that would result from a decameric assembly. In comparison, the larger soluble oligomers eluted in the void volume and would occupy a volume greater than that for a protein corresponding to 700 000 daltons. DLS experiments clearly showed that the larger oligomer of HTB1E and HTB1D exist as a mixture of large oligomers with an average diameter of 34 and 25 nm, respectively. Thus, the DLS and size-exclusion data together support the existence of very large soluble oligomers that are similar to those of other naturally occurring soluble oligomers seen in a variety of proteins implicated in amyloidosis. Reinjection of the purified oligomers showed that the two oligomeric species are not prone to reequilibration over a week. Furthermore, concentration-dependent refolding studies also suggest that the two oligomeric species are not in equilibrium under physiological conditions and possibly arise from distinct folding pathways.

The smaller of these oligomers, HTB1Ep2 and HTB1Dp2, were found to be significantly less structured than the larger oligomers as evidenced by circular dichroism spectroscopy. Whereas the larger soluble oligomeric species, HTB1Ep1 and HTB1Dp1, were found to be more structured, corresponding to β-sheet-rich secondary structure. These oligomers, HTB1Ep1 and HTB1Dp1, showed a relative increase in intensity at 218 nm over 208 nm when compared to the parent HTB1, suggesting gain of β-sheet structure brought about by the core mutation. Fluorescence emission spectra of the single tryptophan residue present in HTB1 and in the two mutants, HTB1E and HTB1D, confirmed the significant structural rearrangement observed in the CD experiments. The tryptophan fluorescence of both oligomeric species of HTB1E and HTB1D was quenched in the mutants compared to the parent HTB1. The smaller decameric oligomers, HTB1Ep2 and HTB1Dp2, showed a center of spectral mass that was within experimental error to that of the parent HTB1. In comparison the larger oligomers, HTB1Ep1 and HTB1Dp1 showed a center of spectral mass that was significantly blue-shifted by 4 nm. This spectral shift suggests a distinctly different, possibly buried, tryptophan environment for the larger oligomeric species in comparison to the smaller oligomers and the parent HTB1.

To provide comparison to known β-sheet-rich oligomers, we utilized histological dyes to probe whether these novel oligomeric species possessed amyloid like β-sheet structural arrangements. Both of the large oligomers, HTB1Ep1 and HTB1Dp1 displayed strong thioflavin T binding over that of the parent HTB1, suggesting that the large soluble oligomers are not amorphous aggregates but ordered structures, as shown for the E7 protein of HPV16 (*10*) and with molten globule aggregates of β-lactoglobulin (*36*). Even though thioflavin T fluorescence is often associated with amyloid fibers, no fibrillar structures were observed by electron microscopy (Supporting Information) in either HTB1E or HTB1D, demonstrating that thioflavin T can bind nonfibrillar β-sheet structures. To validate the results from thioflavin T-dependent fluorescence, the Congo Red binding ability of the large oligomers was also investigated. Both of the large oligomers, HTB1Ep1 and HTB1Dp1, displayed significant Congo Red binding and thus point to a soluble β-sheet-rich aggregate structure.

The large soluble oligomers of HTB1Dp1 (25.2 nm) and HTB1Ep1 (34.4 nm), if modeled as a solid sphere, will correspond to assemblies of 600 monomers and 1500 monomers, respectively. Alternatively, if the soluble oligomers form a hollow single-layer sphere, the HTB1Dp1 oligomers will correspond to an assembly of 300 monomers, whereas the HTB1Ep1 oligomers will correspond to an assembly of 600 monomers.

The observed single mutations in the HTB1 domain that lead to two distinct oligomeric species are very interesting from a protein design and folding perspective, where most single mutations in protein cores, although often destabilizing, have little effect upon tertiary structure (*41*−*44*). However, recent examples of dramatic structural switches to stable structures by single-point mutations have been observed in the B1 domain of protein G (*30*), protein L (*28*), and in the Arc repressor mutants (*45*), although perhaps none of these examples is as dramatic as the present case. Future experiments will probe the effect of pH and the origin of the selective advantage of these remarkable mutants of HTB1.

CONCLUSION

In summary, we have demonstrated that single-point core mutations in a monomeric thermostable protein of the ubiquitin fold can result in significant structural rearrangement that results in two distinct species, comprising a

structurally reorganized oligomer of 5 nm dimensions and of large spherical oligomers of 25−40 nm diameter. Our results suggest that the formation of alternately folded oligomers and large spherical oligomers may be a general feature of proteins with a partially destabilized native fold. The observed soluble oligomers are also interesting from the perspective of biomaterials design, where many different classes of self-assembling biological assemblies are under study for materials templating and construction (*46*−*49*). The soluble oligomers that we have characterized are reminiscent of many naturally occurring heterogeneous self-assembled structures that have been observed in β-amyloid and related fibril forming proteins, small heat shock proteins, RING-domain proteins, viral E7 protein, amelogenin, and β-lactoglobulin. Thus, this emerging class of large spherical oligomers may very well present alternate low energy minima on the protein folding landscape similar to the self-assembled β-sheet-rich fibrillar structures observed in diverse proteins (*3*).

ACKNOWLEDGMENT

We thank Matt Cordes, Rajan Ramaswami, Reena Zutshi, the Ghosh group, and our reviewers for insightful comments. We thank Tom Baldwin, Mike Cusanovich, and Katrina Miranda for the use of their instruments.

SUPPORTING INFORMATION AVAILABLE

Data describing SDS dependence of oligomers, IgG binding, gel filtration experiments, and transmission electron microscopy. This material is available free of charge via the Internet at http://pubs.acs.org.

REFERENCES

1. Lindsey, J. S. (1991) Self-Assembly in Synthetic Routes to Molecular Devices − Biological Principles and Chemical Perspectives − a Review, *New J. Chem. 15*, 153−180.
2. DeGrado, W. F., Wasserman, Z. R., and Lear, J. D. (1989) Protein design, a minimalist approach, *Science 243*, 622−628.
3. Dobson, C. M. (2003) Protein folding and misfolding, *Nature 426*, 884−890.
4. Rochet, J. C., and Lansbury, P. T. (2000) Amyloid fibrillogenesis: themes and variations, *Curr. Opin. Struct. Biol. 10*, 60−68.
5. Haley, D. A., Horwitz, J., and Stewart, P. L. (1998) The small heat-shock protein, alpha B-crystallin, has a variable quaternary structure, *J. Mol. Biol. 277*, 27−35.
6. Moradian-Oldak, J., Leung, W., and Fincham, A. G. (1998) Temperature and pH-dependent supramolecular self-assembly of amelogenin molecules: A dynamic light-scattering analysis, *J. Struct. Biol. 122*, 320−327.
7. Moradian-Oldak, J., Paine, M. L., Lei, Y. P., Fincham, A. G., and Snead, M. L. (2000) Self-assembly properties of recombinant engineered amelogenin proteins analyzed by dynamic light scattering and atomic force microscopy, *J. Struct. Biol. 131*, 27−37.
8. Kentsis, A., Gordon, R. E., and Borden, K. L. B. (2002) Self-assembly properties of a model RING domain, *Proc. Natl. Acad. Sci. U.S.A. 99*, 667−672.
9. Kentsis, A., Gordon, R. E., and Borden, K. L. B. (2002) Control of biochemical reactions through supramolecular RING domain self-assembly, *Proc. Natl. Acad. Sci. U.S.A. 99*, 15404−15409.
10. Alonso, L. G., Garcia-Alai, M. M., Smal, C., Centeno, J. M., Iacono, R., Castano, E., Gualfetti, P., and de Prat-Gay, G. (2004) The HPV 16 E7 viral oncoprotein self-assembles into defined spherical oligomers, *Biochemistry 43*, 3310−3317.
11. Yong, W., Lomakin, A., Kirkitadze, M. D., Teplow, D. B., Chen, S. H., and Benedek, G. B. (2002) Structure determination of micelle-like intermediates in amyloid beta-protein fibril assembly by using small angle neutron scattering, *Proc. Natl. Acad. Sci. U.S.A. 99*, 150−154.
12. Tycko, R. (2004) Progress towards a molecular-level structural understanding of amyloid fibrils, *Curr. Opin. Struct. Biol. 14*, 96−103.
13. Walsh, D. M., Klyubin, I., Fadeeva, J. V., Cullen, W. K., Anwyl, R., Wolfe, M. S., Rowan, M. J., and Selkoe, D. J. (2002) Naturally secreted oligomers of amyloid beta protein potently inhibit hippocampal long-term potentiation in vivo, *Nature 416*, 535−539.
14. Lomakin, A., Chung, D. S., Benedek, G. B., Kirschner, D. A., and Teplow, D. B. (1996) On the nucleation and growth of amyloid beta-protein fibrils: Detection of nuclei and quantitation of rate constants, *Proc. Natl. Acad. Sci. U.S.A. 93*, 1125−1129.
15. Kayed, R., Head, E., Thompson, J. L., McIntire, T. M., Milton, S. C., Cotman, C. W., and Glabe, C. G. (2003) Common structure of soluble amyloid oligomers implies common mechanism of pathogenesis, *Science 300*, 486−489.
16. Smith, C. K., Withka, J. M., and Regan, L. (1994) A Thermodynamic Scale for the Beta-Sheet Forming Tendencies of the Amino-Acids, *Biochemistry 33*, 5510−5517.
17. Smith, C. K., and Regan, L. (1995) Guidelines for Protein Design − the Energetics of Beta-Sheet Side-Chain Interactions, *Science 270*, 980−982.
18. Dalal, S., Balasubramanian, S., and Regan, L. (1997) Protein alchemy: Changing beta-sheet into alpha-helix, *Nat. Struct. Biol. 4*, 548−552.
19. Regan, L. (1993) The Design of Metal-Binding Sites in Proteins, *Annu. Rev. Biophys. Biomol. Struct. 22*, 257−281.
20. Minor, D. L., and Kim, P. S. (1994) Measurement of the Beta-Sheet-Forming Propensities of Amino-Acids, *Nature 367*, 660−663.
21. Minor, D. L., Jr., and Kim, P. S. (1994) Context is a major determinant of beta-sheet propensity, *Nature 371*, 264−267.
22. Gronenborn, A. M., Filpula, D. R., Essig, N. Z., Achari, A., Whitlow, M., Wingfield, P. T., and Clore, G. M. (1991) A novel, highly stable fold of the immunoglobulin binding domain of streptococcal protein G, *Science 253*, 657−661.
23. Distefano, M. D., Zhong, A., and Cochran, A. G. (2002) Quantifying beta-sheet stability by phage display, *J. Mol. Biol. 322*, 179−188.
24. McCallister, E. L., Alm, E., and Baker, D. (2000) Critical role of beta-hairpin formation in protein G folding, *Nat. Struct. Biol. 7*, 669−673.
25. Achari, A., Hale, S. P., Howard, A. J., Clore, G. M., Gronenborn, A. M., Hardman, K. D., and Whitlow, M. (1992) 1.67-A X-ray structure of the B2 immunoglobulin-binding domain of streptococcal protein G and comparison to the NMR structure of the B1 domain, *Biochemistry 31*, 10449−10457.
26. Gronenborn, A. M., Filpula, D. R., Essig, N. Z., Achari, A., Whitlow, M., Wingfield, P. T., and Clore, G. M. (1991) A novel, highly stable fold of the immunoglobulin binding domain of streptococcal protein G, *Science 253*, 657−661.
27. Frank, M. K., Dyda, F., Dobrodumov, A., and Gronenborn, A. M. (2002) Core mutations switch monomeric protein GB1 into an intertwined tetramer, *Nat. Struct. Biol. 9*, 877−885.
28. Byeon, I. J. L., Louis, J. M., and Gronenborn, A. M. (2003) A protein contortionist: Core mutations of GB1 that induce dimerization and domain swapping, *J. Mol. Biol. 333*, 141−152.
29. Bennett, M. J., Schlunegger, M. P., and Eisenberg, D. (1995) 3d Domain Swapping − a Mechanism for Oligomer Assembly, *Protein Sci. 4*, 2455−2468.
30. O'Neill, J. W., Kim, D. E., Johnsen, K., Baker, D., and Zhang, K. Y. J. (2001) Single-site mutations induce 3D domain swapping in the B1 domain of protein L from Peptostreptococcus magnus, *Structure 9*, 1017−1027.
31. Ramirez-Alvarado, M., Merkel, J. S., and Regan, L. (2000) A systematic exploration of the influence of the protein stability on amyloid fibril formation in vitro, *Proc. Natl. Acad. Sci. U.S.A. 97*, 8979−8984.
32. Ramirez-Alvarado, M., and Regan, L. (2002) Does the location of a mutation determine the ability to form amyloid fibrils? *J. Mol. Biol. 323*, 17−22.
33. Rajagopal, S., Meza-Romero, R., and Ghosh, I. (2004) Dual surface selection methodology for the identification of thrombin binding

epitopes from hotspot biased phage-display libraries, *Bioorg. Med. Chem. Lett. 14*, 1389−1393.
34. Sloan, D. J., and Hellinga, H. W. (1999) Dissection of the protein G B1 domain binding site for human IgG Fc fragment, *Protein Sci. 8*, 1643−1648.
35. Sloan, D. J., and Hellinga, H. W. (1998) Structure-based engineering of environmentally sensitive fluorophores for monitoring protein−protein interactions, *Protein Eng. 11*, 819−823.
36. Carrotta, R., Bauer, R., Waninge, R., and Rischel, C. (2001) Conformational characterization of oligomeric intermediates and aggregates in beta-lactoglobulin heat aggregation, *Protein Sci. 10*, 1312−1318.
37. Chin, J. W., and Schepartz, A. (2001) Design and evolution of a miniature bcl-2 binding protein, *Angew. Chem., Int. Ed. 40*, 3806−3809.
38. Xu, G. F., Wang, W. X., Groves, J. T., and Hecht, M. H. (2001) Self-assembled monolayers from a designed combinatorial library of de novo beta-sheet proteins, *Proc. Natl. Acad. Sci. U.S.A. 98*, 3652−3657.
39. Byeon, I. J. L., Louis, J. M., and Gronenborn, A. M. (2004) A captured folding intermediate involved in dimerization and domain-swapping of GB1, *J. Mol. Biol. 340*, 615−625.
40. Kuhlman, B., O'Neill, J. W., Kim, D. E., Zhang, K. Y. J., and Baker, D. (2001) Conversion of monomeric protein L to an obligate dimer by computational protein design, *Proc. Natl. Acad. Sci. U.S.A. 98*, 10687−10691.
41. Lim, W. A., and Sauer, R. T. (1989) Alternative Packing Arrangements in the Hydrophobic Core of Lambda-Repressor, *Nature 339*, 31−36.
42. Sandberg, W. S., and Terwilliger, T. C. (1991) Energetics of Repacking a Protein Interior, *Proc. Natl. Acad. Sci. U.S.A. 88*, 1706−1710.
43. Baldwin, E. P., Hajiseyedjavadi, O., Baase, W. A., and Matthews, B. W. (1993) The Role of Backbone Flexibility in the Accommodation of Variants That Repack the Core of T4-Lysozyme, *Science 262*, 1715−1718.
44. Cordes, M. H. J., Davidson, A. R., and Sauer, R. T. (1996) Sequence space, folding and protein design, *Curr. Opin. Struct. Biol. 6*, 3−10.
45. Cordes, M. H. J., Burton, R. E., Walsh, N. P., McKnight, C. J., and Sauer, R. T. (2000) An evolutionary bridge to a new protein fold, *Nat. Struct. Biol. 7*, 1129−1132.
46. Zhou, M., Bentley, D., and Ghosh, I. (2004) Helical supramolecules and fibers utilizing leucine zipper-displaying dendrimers, *J. Am. Chem. Soc. 126*, 734−735.
47. Vauthey, S., Santoso, S., Gong, H. Y., Watson, N., and Zhang, S. G. (2002) Molecular self-assembly of surfactant-like peptides to form nanotubes and nanovesicles, *Proc. Natl. Acad. Sci. U.S.A. 99*, 5355−5360.
48. Yeates, T. O., and Padilla, J. E. (2002) Designing supramolecular protein assemblies, *Curr. Opin. Struct. Biol. 12*, 464−470.
49. Zhang, S. G., Marini, D. M., Hwang, W., and Santoso, S. (2002) Design of nanostructured biological materials through self-assembly of peptides and proteins, *Curr. Opin. Chem. Biol. 6*, 865−871.

BI048197L